Contents lists available at ScienceDirect

Transactions of Nonferrous Metals Society of China

36(2026) 144−155

www.tnmsc.cn

Weakening aging-induced embrittlement via deformation-assisted regulation of isothermal ω precipitation in metastable Ti−15Mo alloy

Fei ZHANG [a,b#], Shi-wei PAN [a,b#], Shun XU [a,b,*], Feng QIAN [a,b], Jiang-kun FAN [c], Qun-bo FAN [a,b,d], Xing-wang CHENG [a,b,**]

[a] School of Materials Science and Engineering, Beijing Institute of Technology, Beijing 100081, China;
[b] National Key Laboratory of Science and Technology on Materials Under Shock and Impact, Beijing 100081, China;
[c] State Key Laboratory of Solidification Processing, Northwestern Polytechnical University, Xi'an 710072, China;
[d] Chongqing Innovation Center, Beijing Institute of Technology, Chongqing 401135, China

Abstract: In order to overcome the embrittlement of metastable titanium alloys caused by the precipitation of ω_{iso} phase during aging, regulation of isothermal ω precipitation was investigated in Ti−15Mo alloy. The results show that the sample is brittle when direct aging (A) is applied at 350 °C for 1 h after solution treatment (ST). If pre-deformation (D) is performed on the ST sample to induce {332} twins and secondary α'' phase, subsequent aging at 350 °C (STDA350) improves the strength to 931 MPa with a good ductility of about 20% maintained. However, when aging is performed at 400 °C or 450 °C (STDA400/450), the strength can be further improved, but the ductility is dramatically reduced. Atomic-scale characterizations show that the partial collapse of ω phase in the STDA350 sample effectively eliminates aging-induced embrittlement, but complete collapse leads to poor ductility in the STDA400/450 sample.

Keywords: room-temperature mechanical property; structural collapse; ω phase; aging-induced embrittlement; Ti−15Mo alloy

1 Introduction

Metastable β type titanium alloys have been used in a wide range of aerospace, biomedicine and energy industries due to their high specific strength, low elastic modulus, and excellent corrosion resistance [1−3]. The tensile properties of the β titanium alloys have been shown to be significantly dependent on the deformation mode as a function of the stability of the β phase, which is controlled by the content and type of alloying elements [4,5]. With the increase of β phase stability, the deformation is alternately dominated by stress-induced martensite and ω phase [6,7], {332}⟨113⟩ twinning [8−11], {112}⟨111⟩ twinning [8,12], and dislocation gliding [8,13]. Transformation-induced plasticity (TRIP) and/or twinning-induced plasticity (TWIP) effects are introduced to achieve an excellent uniform elongation of above 20%, but usually result in a low yield strength generally below 600 MPa [13−15]. In order to increase the yield strength and maintain high work hardening rate for expanding the application of metastable titanium alloys, considerable efforts have been recently devoted to adjusting alloy composition for purposely activating one or multiple specific deformation modes. For example, minor alloying of Fe element into Ti−15Mo has successfully increased the yield strength to 837 MPa, but deteriorates the

Fei ZHANG and Shi-wei PAN contributed equally to this work

Corresponding author: *Shun XU, Tel: +86-10-68911144, E-mail: shunxu@bit.edu.cn;
**Xing-wang CHENG, Tel: +86-10-68913951, E-mail: chengxw@bit.edu.cn

https://doi.org/10.1016/S1003-6326(25)66954-8
Received 24 April 2024; accepted 10 January 2025

uniform elongation seriously [16]. A novel Ti−7Mo−3Cr alloy is designed to couple two twinning systems in the early deformation, achieving a yield strength of 695 MPa and a substantial uniform elongation of 33.3% [17].

Solution treatment ($>T_\beta$) followed by water quench is usually applied in metastable β-Ti alloys in order to obtain complete β-grains with the presence of dense athermal ω phase (ω_{ath}) formed via a displacive phase transformation [18]. During aging at a low temperature range of 150−475 °C, ω_{ath} can further evolve into the isothermal ω phase (ω_{iso}) by a diffusion-controlled process, resulting in uniformly dispersed ω precipitates in β matrix [19,20], but the ductility is deteriorated in the transition from ω_{ath} precipitates to ω_{iso} ones [21]. Since first discovered in Ti−8Cr (wt.%) alloy [22], ω phase has attracted extensive attention due to its significant strengthening effect in β type titanium alloys. To utilize the strengthening effect of ω phase and avoid the embrittlement transition, low temperature aging at 150 °C for 60 s has been reported to effectively increase the yield strength of Ti−12Mo alloy from 480 to 730 MPa with the initial ductility maintained (~40%) [21]. When aging at 475 °C for 48 h, ellipsoidal coarse ω particles (70−90 nm) are developed in Ti−12Mo alloy with a high ultimate tensile strength of 1073 MPa (~550 MPa at solution treated (ST) state) achieved, but a rather limited ductility (<5%) [23]. When Ti−15Mo is aged at 300 °C for 1 h, a high yield strength of 985 MPa is obtained with a total elongation of 16%, but this results in fast necking after yielding [24]. The strengthening effect of the ω_{iso} is attributed to its ability to increase the critical resolved shear stress (CRSS) of stress-induced martensite (SIM), α'', twinning and dislocation gliding [25,26]. Serious embrittlement transition seems to result from the suppression of TRIP/TWIP and dislocation movement [25,27,28].

A combination of {332} twins and ω_{iso} phase provides a possible method to achieve the balance of strength and ductility [29]. Increasing the direct aging temperature after solution treatment (STA) promotes the formation of ω_{iso} phase and improves the strength, but results in the loss of ductility [30], which is attributed to the precipitation-induced transformation of deformation mechanisms from twinning to slip [31,32]. To overcome the sacrifice of ductility, pre-deformation is applied before aging (STDA). The STDA sample shows improved strength while maintaining good ductility. Compared to the STA sample, the enhanced uniform elongation of the STDA sample results from the extra nucleation sources for further twinning mechanism provided by the pre-deformation introduced mechanical twins [30], which help to retard the occurrence of early necking [31]. However, increasing the aging temperature after pre-deformation results in the dramatic loss of ductility, indicating the brittle-to-ductile-to-brittle transitions that are achieved by deformation-regulated precipitation. In particular, few reports have been found on the underlying mechanism. The primary factors governing the brittle-to-ductile-to-brittle transformation still remain inadequately understood. In this work, atomic-scale observations show that the partial collapse of deformation-regulated precipitation of ω_{iso} phase at lower aging temperature effectively eliminates the aging-induced embrittlement, but aging at higher temperatures results in complete collapse of ω_{iso} phase. Therefore, this work provides useful insights of regulating the precipitation of isothermal ω phase to achieve the balance of mechanical properties in metastable titanium alloys.

2 Experimental

Ti−15Mo (wt.%) alloy ingots with a purity of 99.99% were prepared by arc melting of pure Ti and Mo metals in Ar atmosphere. The ingot was melted several times to ensure compositional homogeneity and then cooled in an electric arc furnace. After rolling, the Ti−15Mo alloy with a size of 100 mm × 100 mm × 50 mm was ST at 900 °C for 1 h and then quenched in water to room temperature. Flat dog-bone-shaped specimens for tension with a thickness of 1 mm and a gauge section of 5 mm × 1.5 mm were machined from the ST block by using electrical discharge machining. Then, two different treatment regimes, including direct aging and post-deformation aging, were applied. More specifically, STA350 and STA400 indicate direct aging at 350 and 400 °C for 1 h, respectively. STD denotes deformation with an engineering strain of 5%. STDA350, STDA400 and STDA450 indicate post-deformation aging at

350, 400 and 450 °C for 1 h, respectively. All heat treatments were carried out with the samples sealed in quartz tube. Finally, the designed samples were subjected to tensile tests on a Zwick Z2.5 TH system with a laser extensometer at a quasi-static strain rate of 1×10^{-3} s^{-1}. Each test was repeated for three times.

To characterize the microstructure evolution, specimens for electron backscatter diffraction (EBSD) mapping were ground using SiC paper from 600# to 3000# grit, followed by electrolytic polishing treatment in a solution of 10% perchloric acid, 30% 2-butoryethanol and 60% methanol. EBSD was performed on a field emission gun scanning electron microscope (Thermo Fisher Apreo apparatus), which was operated at 20 kV with a step size of 2 μm for detection of grain size and deformation twins. EBSD data were analyzed using HKL's CHANNEL5 software. The thin foils from the samples were twin-jet electropolished for the transmission electron microscopy (TEM) characterization, which was performed on a transmission electron microscope (Talos F200X G2) to obtain the dark field (DF) images, selected area diffraction (SAED) patterns, high resolution (HR) TEM images and high-angle annular dark field (HAADF) images. TEM data were analyzed by using Digital Micrograph software.

3 Results

3.1 Mechanical response

Figure 1 shows the tensile engineering stress−strain curves of samples. The yield strength (YS), ultimate tensile strength (UTS) and fracture elongation (FE) acquired from the curves are summarized in Table 1. The initial ST sample has YS and UTS of 414 and 708 MPa, respectively, with a high FE of 41.2%. After pre-deformation, the YS of the STD sample increases to 534 MPa, the FE slightly decreases to 37.1%, while the UTS keeps almost unchanged. It can be identified that both ST and STD samples exhibit remarkable work-hardening behavior during tensile test, indicating TWIP and/or TRIP effects. In contrast, a direct aging (350 °C, 1 h) after solution treatment increases the YS and UTS of STA350 sample to 1039 MPa and 1052 MPa, respectively, but a decreased FE of 9.9% is obtained with a strain-softening phenomenon after the yielding point. Besides, increasing direct aging temperature to 400 °C further deteriorates the ductility to 0% and causes the early fracture of STA400 sample. Therefore, direct aging improves the strength but causes serious damage to the plasticity of the material.

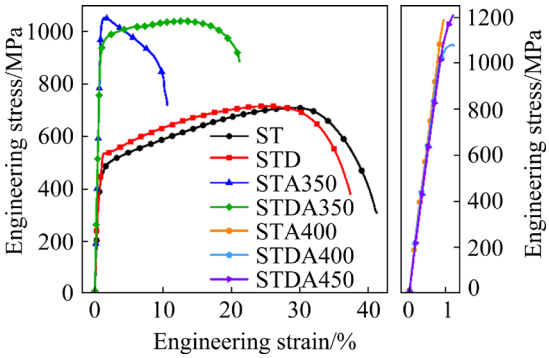

Fig. 1 Tensile engineering stress−strain curves of Ti−15Mo alloy after different processes

Table 1 Mechanical properties of Ti−15Mo alloy after different processes

Sample	Regime		Tensile property		
	Deformation strain/%	Aging	YS/MPa	UTS/MPa	FE/%
ST	−	−	414	708	41.2
STD	5	−	534	712	37.1
STA350	−	350 °C, 1 h	1039	1052	9.9
STDA350	5	350 °C, 1 h	931	1039	21.0
STA400	−	400 °C, 1 h	1188	1188	0
STDA400	5	400 °C, 1 h	1072	1080	0.3
STDA450	5	450 °C, 1 h	1207	1207	0

Interestingly, the STDA350 sample, exhibits significantly high YS and UTS values of 931 MPa and 1039 MPa, respectively. Moreover, this sample achieves an excellent tensile plasticity of 21%, which is double that of the STA350 sample, indicating that deformation-assisted aging can overcome the typical strength−ductility tradeoff. As the aging temperature further increases, detrimental embrittlement occurs. In Fig. 1, the YS of STDA400 and STDA450 falls in the range above 1000 MPa, whereas the FE becomes almost undetectable. Therefore, weakening the aging-induced embrittlement via deformation-assisted regulation of precipitation shows temperature-dependence.

3.2 Microstructural evolution

Figure 2 shows the microstructure of solution-treated Ti−15Mo sample. A complete equiaxed β-grain structure can be identified in the EBSD inverse pole figure (IPF) map (Fig. 2(a)). The size distribution with an average diameter of 140 μm can be determined in Fig. 2(b). In addition, TEM dark-field (DF) image in Fig. 2(c) shows the presence of dense hexagonal ω_{ath} in the β-matrix, and the corresponding SAED pattern taken along $[\bar{1}13]_\beta$ zone axis in Fig. 2(d) confirms the $\langle\bar{1}13\rangle_\beta$ // $\langle11\bar{2}3\rangle_\omega$ and $\langle110\rangle_\beta$// $\langle10\bar{1}\bar{1}\rangle_\omega$ orientation relationship.

For the STA400 sample, the average size of β-grains increases to ~151 μm (Figs. 3(a, b)). This variation could be ascribed to the insufficient statistical counts by EBSD, since the size of β grains mainly depends on the treatment regimes above the β-transus temperature [33]. It is also suggested that most of the ω precipitates have experienced a transition from athermal to isothermal ones during direct aging at 400 °C. Figure 3(c) shows the distribution of elliptical ω_{iso} phase in the β matrix after aging at 400 °C, as observed in STA400 sample. Generally, the ω phase is composed of four variants, namely ω_1, ω_2, ω_3 and ω_4. Since the precipitation is thermally activated, they equivalently distribute along four close-packed $\langle111\rangle_\beta$ orientations [34−36]. Along the specific $[011]_\beta$ zone axis, the spots of ω_1 and ω_2 variants are visible, while the spots of ω_3 and ω_4 variants are overlapped with β-reflections and thus cannot be identified [37]. TEM DF images of the ω_1 and ω_2 variants are shown in Figs. 3(d, e), respectively. The ω precipitates are visualized as elliptical particles and the direction of the elliptic major axis is the same, as illustrated in Fig. 3(f).

The EBSD IPF map in Fig. 4(a) reveals the presence of band structures induced by an engineering strain of 5%, which are identified as {332} twins by misorientation profile in Fig. 4(b). TEM characterizations are performed on the STD sample to explore the microstructure after deformation, as displayed in Figs. 4(c−i). The TEM DF image and the corresponding SAED pattern in

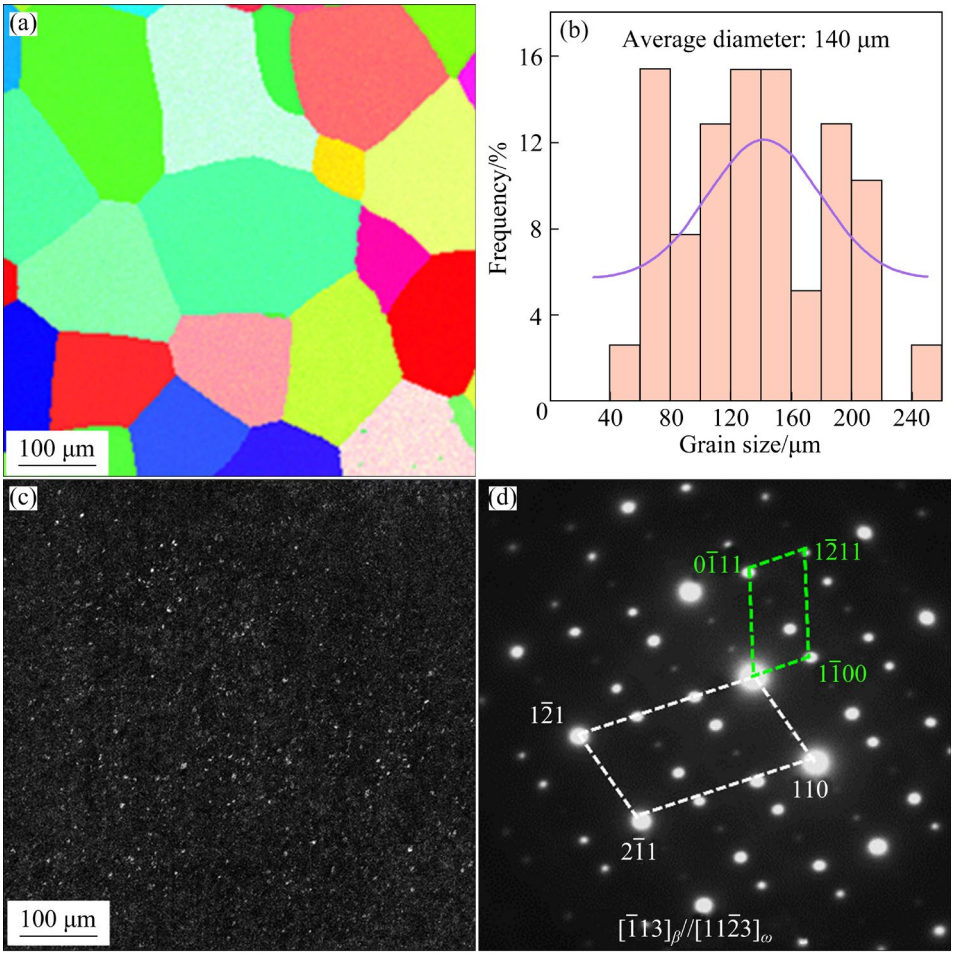

Fig. 2 EBSD and TEM micrographs of ST sample: (a) IPF map; (b) Statistical histogram for β grain sizes; (c) TEM DF micrograph of ω phase; (d) Corresponding SAED pattern

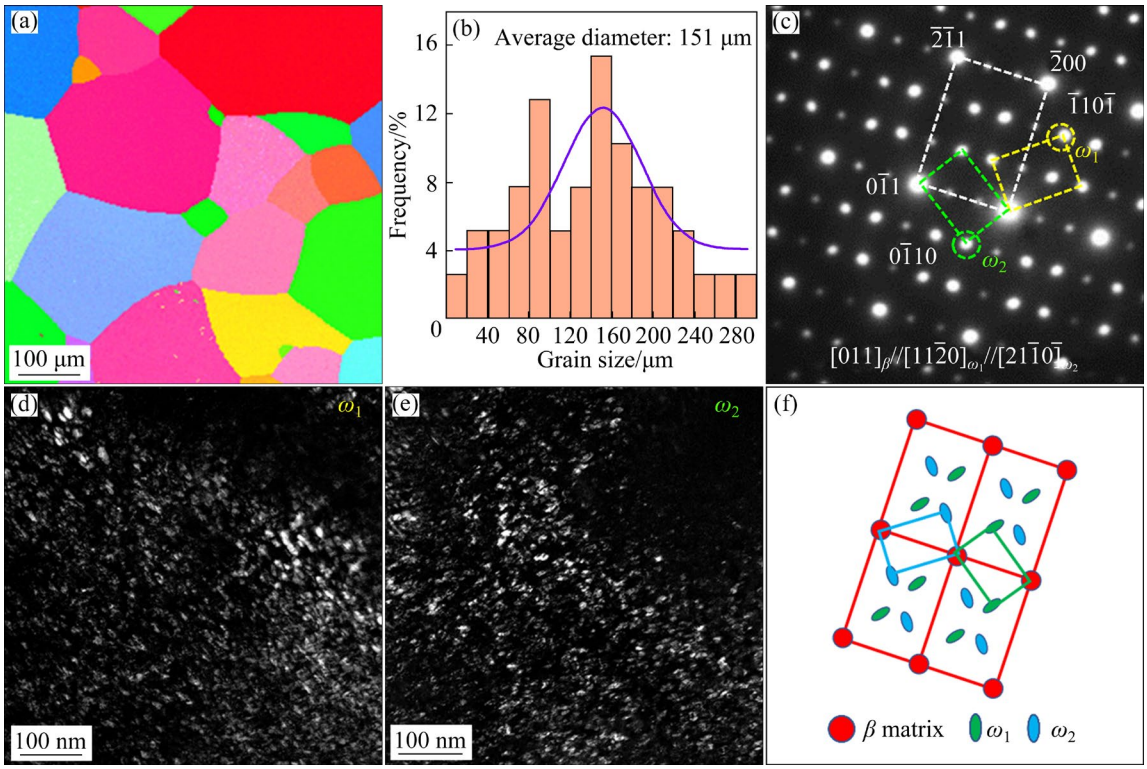

Fig. 3 EBSD and TEM micrographs of STA400 sample: (a) IPF map; (b) Statistical histogram for β grain sizes; (c) SAED pattern; (d, e) TEM DF images of ω phase; (f) Distribution schematic diagram of ω_1 and ω_2

Fig. 4(c) show that the ω_{ath} phase still remains in the β matrix after deformation. The band structure with a width of ~1.5 μm in Fig. 4(d) is further identified as the {332} twin by the SAED pattern in Fig. 4(e) and HRTEM analysis in Fig. 4(f). In addition, extra secondary bands are observed within {332} twin, and are parallel to each other, as seen in Fig. 4(d). These bands can be identified to be α'' martensite as evidenced by the diffraction pattern collected from blue circle region. It is indicated that there is no ω precipitation in these α'' martensitic bands, as shown in Figs. 4(h, i). These results are in good agreement with the findings in metastable β-Ti alloys that the relatively low β-stability results in the stress-induced $\beta \rightarrow \alpha''$ martensitic transformation [38,39], which is preferred to nucleate at β-twin boundaries [38]. The transformation is known to be beneficial for maintaining high strain-hardening and an excellent uniform tensile ductility as reported in Ti−10V−2Fe−3Al alloy [40].

Figure 5 displays EBSD and TEM results of the STDA350, STDA400 and STDA450 samples. The misorientation angle of 50° reveals that the aging does not change the structure of {332} deformation twins. The corresponding TEM DF images and diffraction patterns indicate the ω phase in all three samples. Compared with STD sample, the number density of ω phase particles increases after aging, as shown in the Figs. 5(c−i). It is also shown that the size of ω_{iso} particles gradually increases as the aging temperature increases from 350 to 450 °C. It should be noted that the growth of ω phase particles can develop to tens of nanometers in size and is irreversible [41].

3.3 Fracture morphology

Representative SEM images of the fractured surfaces are shown in Fig. 6 for the fracture mechanisms of the STA350, STDA350 and STDA400 samples. Figures 6(a, b) show that the fractography of the STA350 sample is composed of dimples and a few cleavage facets, indicating the nature of transcrystalline fracture. Comparatively, the STDA350 sample is featured as a high density of dimples homogeneously distributed on the fracture surface, as seen in Figs. 6(c, d). This observation implies that the introduction of pre-deformation before aging can effectively improve the ductility of the sample. However, the

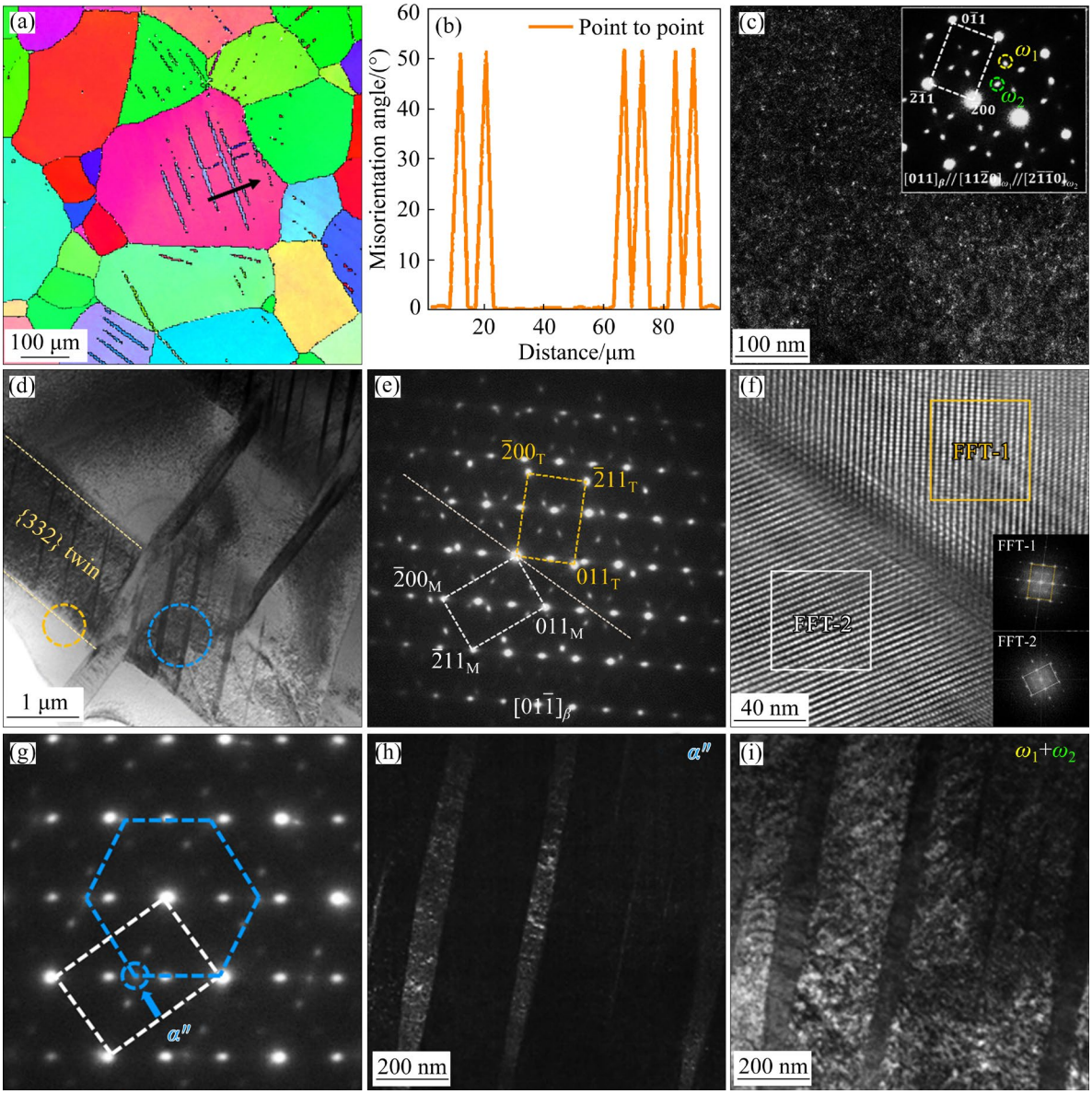

Fig. 4 EBSD and TEM micrographs of STD sample: (a) IPF map; (b) Misorientation profile; (c) TEM DF micrograph of ω phase and corresponding SAED pattern; (d) TEM bright-field micrograph of α'' phase; (e) SAED pattern recorded from golden circle area in (d); (f) HRTEM micrograph and corresponding FFT patterns; (g) SAED pattern recorded from blue circle area in (d); (h) TEM DF micrograph of α'' phase; (i) TEM DF micrograph of ω phase

dominant feature of STDA400 sample as shown in Figs. 6(e, f), is the presence of cleavage facets with a few dimples. This proves the typical cleavage fracture mode, resulting from severe dislocation accumulation along grain boundaries and leading to early micro-cracks [42−44]. This is consistent with the tensile testing that the STDA400 sample has a limited fracture elongation of 0.3%. The results show that deformation-assisted regulation of ω_{iso} precipitation is effective to overcome the embrittlement, but the selection of appropriate temperatures for the subsequent aging is essentially required.

Based on the experimental results, pre-strain prior aging can effectively help to overcome the strength and ductility tradeoff in metastable β Ti−15Mo alloy, whereas the effect is highly temperature-dependent. More specifically, the introduction of 5% pre-strain before undergoing 350 °C artificial aging induces a ductile fracture and thus achieves high strengths (YS of 931 MPa, UTS of 1039 MPa) and good ductility (EL of 21%) during tensile testing. In contrast, a simple direct aging at the same temperature usually leads to a

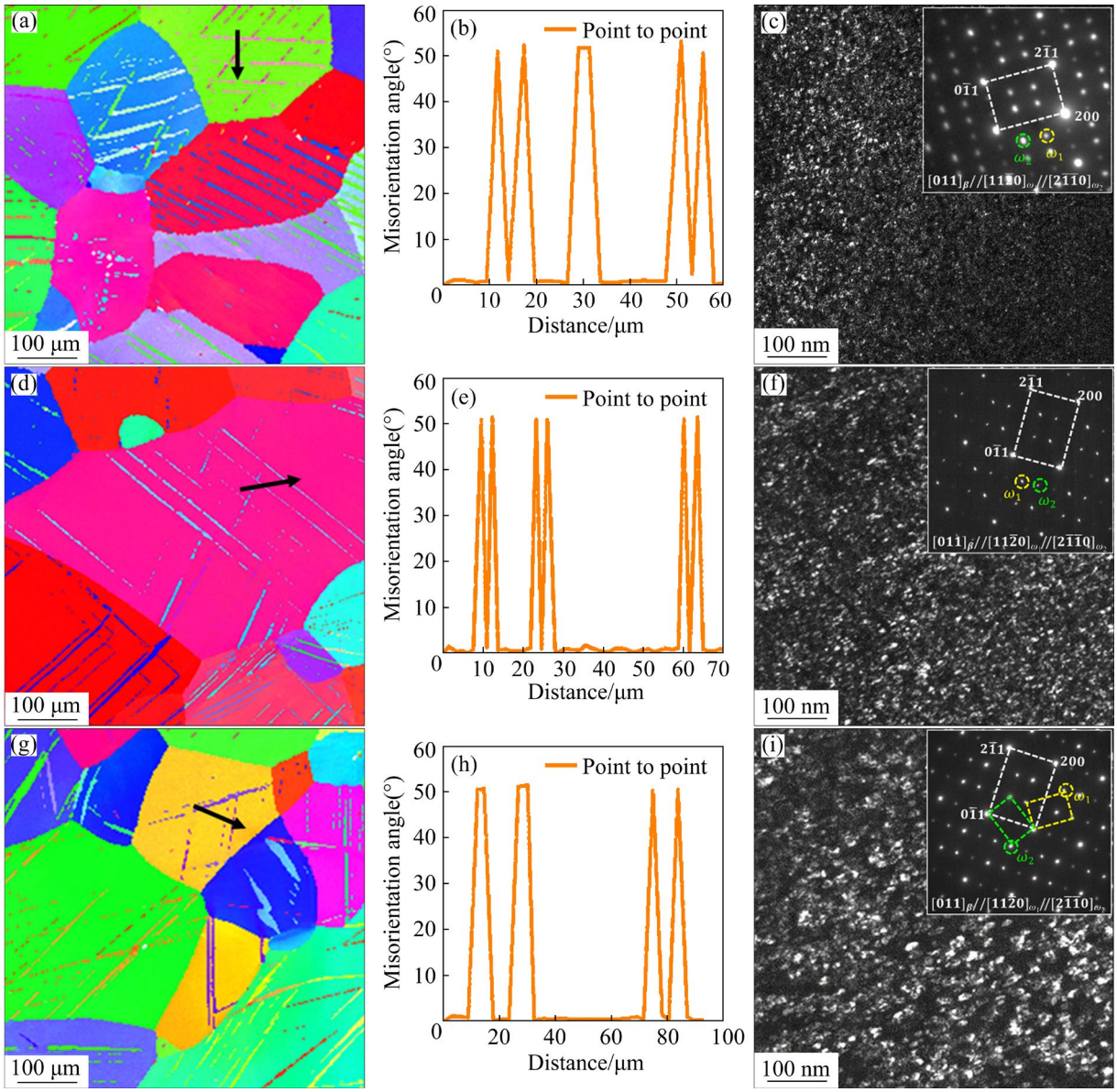

Fig. 5 EBSD and TEM micrographs of (a−c) STDA350 sample, (d−f) STDA400 sample and (g−i) STDA450 sample: (a, d, g) IPF maps; (b, e, h) Misorientation profiles; (c, f, i) TEM DF images of ω phase and corresponding SAED patterns

hybrid fracture with a much lower ductility of 9.9% (Fig. 1). Comparatively, the higher aging temperature of 350 °C achieved in this work effectively broadens the service temperature range of Ti−15Mo alloy with a good balance of strength and plasticity, especially when compared to directly-aged alloys. Nevertheless, an obvious ductile−brittle transition occurs as the aging temperature increases from 350 to 400 °C. For the STDA400 and STDA450 samples, severe embrittlement with negligible elongations occurs at higher aging temperatures following pre-deformation.

3.4 Evolution of ω phase

The experimental results demonstrate that the mechanical properties and fracture characteristics of the samples are significantly influenced by the deformation-regulated precipitation of ω phase. The high-resolution TEM investigations were conducted to examine the microstructural features. In Fig. 7(a), a typical example of the ω phase with a largely collapsed structure can be observed in the STA350 sample, which exhibits high strength but low ductility (as shown in Fig. 1). When the deformation twins are introduced into the STDA350 sample, most of the ω phase is identified to be partially

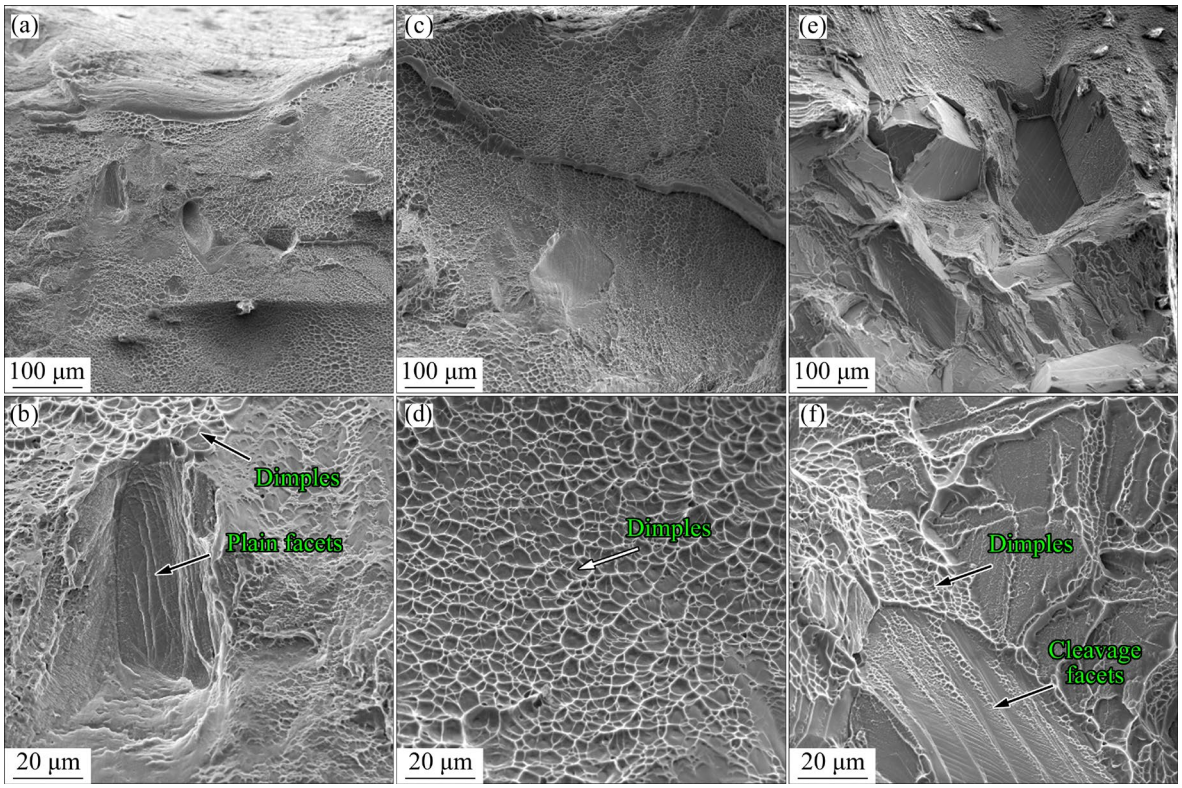

Fig. 6 SEM images showing fractography of samples: (a, b) STA350; (c, d) STDA350; (e, f) STDA400

collapsed, with the shear distance between 0 and 1/12[111], as shown in Fig. 7(b). As a result, a considerable ductility of 21% is maintained (Fig. 1). However, as the aging temperature further increases to 400 °C, the complete structural collapse of ω phase is widely observed in the STDA400, with a dramatic decrease in ductility (Fig. 7(c)). This structural collapse of the ω phase is also accompanied by the diffusion of Mo elements from the ω phase to the surrounding β-matrix. The distribution of Mo element in these three samples shown in Figs. 7(d−i) indicates the diffusion behavior of Mo from the ω to β phase. In particular, the line-scanning results in Fig. 7(d) reveal an obvious fluctuation of the Mo element in the STA350 sample, even though the size of the ω particles is still small at this stage. In contrast, a significant number of dislocations appear in the STDA350 sample, and the spheroidization of the ω particles is noticeably reduced. Correspondingly, the distribution of Mo element in the β matrix becomes more uniform. However, in the STDA400 sample, the dimensions of ω particles continue to increase, and more Mo element diffuse from the ω to β phase.

It has been extensively reported that the volume fraction and size of the ω particles improve as the aging temperature increases [19,22,45]. Besides, the self-hardening behavior of the ω precipitates causes the mechanism transition from deformation twinning to dislocation slip [46]. Figure 8 presents a schematic diagram illustrating the degree of structural collapse of the ω phase. Delaying the structural collapse of ω phase effectively leads to an improvement in the ductility of STDA350 sample. However, when the aging temperature after pre-deformation is increased to 400 °C, the ω phase collapses completely, leading to poor ductility. As ω particle size increases, the degree of structural collapse and element partitioning become more pronounced. The accumulation of Mo atoms in β phase significantly enhances phase stability, which in turn inhibits the occurrence of twinning and stress-induced phase transformation [47,48]. This inhibition reduces the ductility of the alloy. Furthermore, a high density of dislocations is homogeneously distributed in the β matrix (Fig. 7(e)). During the aging process at 350 °C, these dislocations serve as the diffusion channels that can quickly “absorb” most of the supersaturated Mo solute atoms, causing Mo segregation at dislocations. As a result, the later

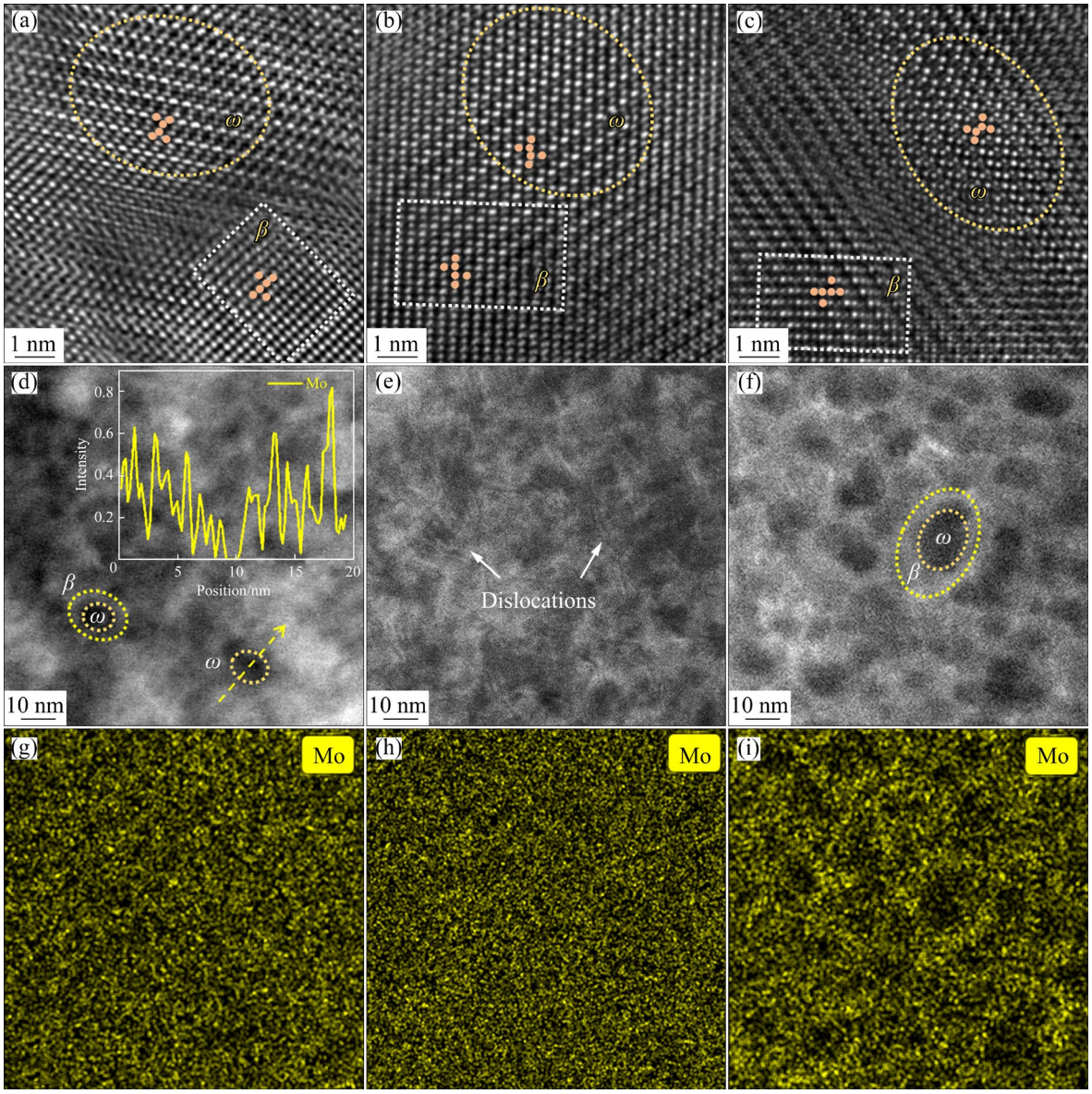

Fig. 7 HRTEM images of (a) STA350, (b) STDA350 and (c) STDA400 samples; HAADF TEM images and corresponding Mo element distributions of (d, g) STA350 sample, (e, h) STDA350 sample and (f, i) STDA400 sample

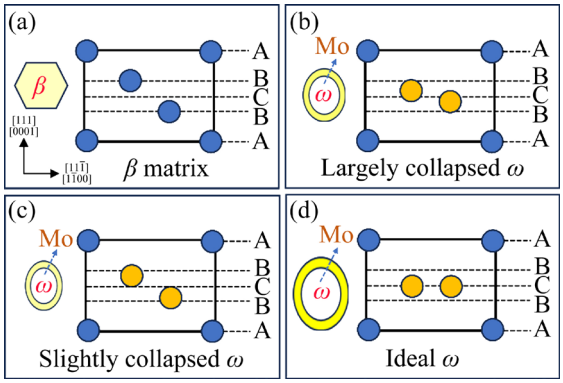

Fig. 8 Schematic diagram of structural collapse and Mo distribution of ω phase in different samples: (a) ST; (b) STA350; (c) STDA350; (d) STDA400

rejection of Mo atoms from ω to the surrounding matrix could be inhibited due to the reduced chemical driving force compared to the STA350 sample. This inhibition results in the suppressed growth of ω_{iso} phases observed in the present study.

4 Conclusions

(1) The strength of Ti−15Mo alloy increases while its plasticity diminishes with an increase in aging temperature during direct aging, which is attributed to the precipitation of the ω phase. The fracture morphology of the sample aged at 350 °C exhibits both ductile and brittle features.

(2) The embrittlement of Ti−15Mo alloy during direct aging at 350 °C can be overcome by pre-deformation before aging, and the sample exhibits significantly high yield strength and ultimate tensile strength of 931 MPa and 1039 MPa, with an excellent tensile plasticity of 21% achieved.

(3) The ability to weaken the aging-induced embrittlement via deformation-assisted regulation of precipitation is temperature-dependent. This phenomenon is related to the structural collapse behavior and Mo element diffusion behavior of the ω precipitates.

CRediT authorship contribution statement

Fei ZHANG: Investigation, Data curation, Visualization, Writing − Original draft; **Shi-wei PAN:** Conceptualization, Methodology, Supervision, Writing − Review & editing; **Shun XU:** Funding acquisition, Resources, Supervision, Writing − Review & editing, Formal analysis; **Feng QIAN:** Investigation, Data curation; **Jiang-kun FAN:** Investigation, Data curation; **Qun-bo FAN:** Writing − Review & editing; **Xing-wang CHENG:** Funding acquisition, Resources, Supervision.

Declaration of competing interest

The authors declare that they have no known competing financial interests or personal relationships that could have appeared to influence the work reported in this paper.

Acknowledgments

The authors are grateful to the financial support from the National Natural Science Foundation of China (No. 52374380) and the China Postdoctoral Science Foundation (Nos. 2023M730234, 2024T171126).

References

[1] CHEN Zhao-qi, XU Li-juan, CAO Shou-zhen, YANG Jian-kai, ZHENG Yun-fei, XIAO Shu-long, TIAN Jing, CHEN Yu-yong. Characterization of hot deformation and microstructure evolution of a new metastable β titanium alloy [J]. Transactions of Nonferrous Metals Society of China, 2022, 32: 1513−1529.

[2] ZHU Yan-yan, CHEN Bo, TANG Hai-bo, CHENG Xu, WANG Hua-ming, LI Jia. Influence of heat treatments on microstructure and mechanical properties of laser additive manufacturing Ti−5Al−2Sn−2Zr−4Mo−4Cr titanium alloy [J]. Transactions of Nonferrous Metals Society of China, 2018, 28: 36−46.

[3] ZHENG Yu-feng, BANERJEE R, FRASER H L. A nano-scale instability in the β phase of dilute Ti−Mo alloys [J]. Scripta Materialia, 2016, 116: 131−134.

[4] XU Sheng-hang, LIU Yong, LIU Bin, WANG Xin, CHEN Zhi-xing. Microstructural evolution and mechanical properties of Ti−5Al−5Mo−5V−3Cr alloy by heat treatment with continuous temperature gradient [J]. Transactions of Nonferrous Metals Society of China, 2018, 28: 273−281.

[5] KOLLI P R, DEVARAJ A. A review of metastable beta titanium alloys [J]. Metals, 2018, 8: 506−546.

[6] CASTANY P, GLORIANT T, SUN Fan, PRIMA F. Design of strain-transformable titanium alloys [J]. Comptes Rendus Physique, 2018, 19: 710−720.

[7] ZHANG Dai-chi, XUE Qun-ji, LEI Jia-feng, MA Yu-jiu, YANG Rui, WANG Chao. Influence of grain size on mechanical responses in beta Ti−12Mo alloy demonstrating concurrent twinning-induced plasticity/transformation-induced plasticity effects [J]. Metallurgical and Materials Transactions, 2018, 49: 3161−3166.

[8] YANG Yi, WU Song-quan, LI Ge-ping, LI Yong-liang, LU Ya-feng, YANG Ke, GE Peng. Evolution of deformation mechanisms of Ti−22.4Nb−0.73Ta−2Zr−l.34O alloy during straining [J]. Acta Materialia, 2010, 58: 2778−2787.

[9] MARTELEUR M, SUN Fan, GLORIANT T, VERMAUT P, JACQUES P, PRIMA F. On the design of new β metastable titanium alloys with improved work hardening rate thanks to simultaneous TRIP and TWIP effects [J]. Scripta Materialia, 2012, 66: 749−752.

[10] ZHOU Zhong-bo, FEI Yue, LAI Min-jie, KOU Hong-chao, CHANG Hui, SHANG Guo-qiang, ZHU Zhi-shou, LI Jin-shan, ZHOU Lian. Microstructure and mechanical properties of new metastable β type titanium alloy [J]. Transactions of Nonferrous Metals Society of China, 2010, 20: 2253−2258.

[11] DANARD Y, SUN Fan, GLORIANT T, FREIHERR I, PIELLARD M, PRIMA F. The influence of twinning on the strain-hardenability in TRIP/TWIP titanium alloys: Role of solute-solution strengthening [J]. Frontiers in Materials, 2020, 7: 240−250.

[12] LAI Min-jie, TASAN C C, ZHANG Jia-li, GRABOWSKI B, HUANG Liang-feng, RAABE D. Origin of shear induced β to ω transition in Ti−Nb-based alloys [J]. Acta Materialia, 2015, 92: 55−63.

[13] SUN Fan, ZHANG Jin-yong, MARTELEUR M, GLORIANT T, VERMAUT P, LELE D, CASTANY P, CURFS C, JACQUES P J, PRIMA F. Investigation of early stage deformation mechanisms in a metastable β titanium alloy showing combined twinning-induced plasticity and transformation-induced plasticity effects [J]. Acta Materialia, 2013, 61: 6406−6417.

[14] VARENNE C, PRIMA F, BROZEK C, BOURGON J, BESSON J, GOURGUES-LORENZON A F. High impact resistance of a TWIP β titanium alloy: Linking the multi-scale deformation and fracture mechanisms [J]. Journal of Materials Science, 2020, 56: 5201−5214.

[15] KWASNIAK P, SUN Fan, MANTRI S, BANERJEE R, PRIMA F. Polymorphic nature of {332}⟨113⟩ twinning mode in BCC alloys [J]. Materials Research Letters, 2022, 10: 334−342.

[16] YAO Kai, MIN Xiao-hua, EMURA S, TSUCHIYA K. Coupling effect of deformation mode and temperature on

tensile properties in TWIP type Ti−Mo alloy [J]. Materials Science and Engineering A, 2019, 766: 138363−138372.

[17] GAO Jun-heng, HUANG Yu-he, GUAN Di-kai, KNOWLES A J, MA Le, DYE D, RAINFORTH W M. Deformation mechanisms in a metastable beta titanium twinning induced plasticity alloy with high yield strength and high strain hardening rate [J]. Acta Materialia, 2018, 152: 301−314.

[18] CAMPANELLI L C, COURY F G, GUO Yao-feng, PEREIRA DA SILVA P S C, KAUFMAN M J, BOLFARINI C. The role of twinning and nano-crystalline ω phase on the fatigue behavior of the metastable β Ti−15Mo alloy [J]. Materials Science and Engineering A, 2018, 729: 323−330.

[19] ZHANG Feng, FENG Jun, XIANG Wei, FU Qiang, YUAN Wu-hua. Enhanced mechanical properties in metastable β titanium alloy via ω-assisted nucleation [J]. Materials Science and Engineering A, 2022, 858: 144082−144094.

[20] XU Tie-wei, ZHANG Shan-shan, ZHANG Feng-shou, KOU Hong-chao, LI Jin-shan. Effect of ω-assisted precipitation on $\beta\rightarrow\alpha$ transformation and tensile properties of Ti−15Mo−2.7Nb−3Al−0.2Si alloy [J]. Materials Science and Engineering A, 2016, 654: 249−255.

[21] SUN Fan, ZHANG Jin-yong, VERMAUT P, CHOUDHURI D, ALAM T, MANTRI S A, SVEC P, GLORIANT T, JACQUES P J, BANERJEE R, PRIMA F. Strengthening strategy for a ductile metastable β titanium alloy using low-temperature aging [J]. Materials Research Letters, 2017, 5: 547−553.

[22] CHEN Kai, FAN Qun-bo, YANG Lin, XU Shun, YAO Jia-hao, GAO Yu, LEI Wei. A novel sequential mechanism associated with stress-induced $\beta\rightarrow\omega\rightarrow\beta+\alpha$ phase transformation in Ti−6Mo−3.5Cr−1Zr titanium alloy [J]. Materials Science and Engineering A, 2022, 849: 143355−143360.

[23] MANTRI S A, CHOUDHURI D, ALAM T, AGEH V, SUN Fan, PRIMA F, BANERJEE R. Change in the deformation mode resulting from beta-omega compositional partitioning in a Ti−Mo alloy: Room versus elevated temperature [J]. Scripta Materialia, 2017, 130: 69−73.

[24] MIN Xiao-hua, EMURA S, NISHIMURA T, ZHANG Ling, TAMILSELVI S, TSUCHIYA K, TSUZAKI K. Effects of α phase precipitation on crevice corrosion and tensile strength in Ti−15Mo alloy [J]. Materials Science and Engineering A, 2010, 576: 1480−1488.

[25] QIAN Bing-nan, MANTRI S A, DASARI S, ZHANG Jin-yong, LILENSTEN L, SUN Fan, VERMAUT P, BANERJEE R, PRIMA F. Mechanisms underlying enhanced strength-ductility combinations in TRIP/TWIP Ti−12Mo alloy engineered via isothermal omega precipitation [J]. Acta Materialia, 2023, 245: 118619−118630.

[26] LAI Min-jie, TASAN C C, RAABE D. Deformation mechanism of ω-enriched Ti−Nb-based gum metal: Dislocation channeling and deformation induced $\omega-\beta$ transformation [J]. Acta Materialia, 2015, 100: 290−300.

[27] LAI Min-jie, LI Tong, RAABE D. ω phase acts as a switch between dislocation channeling and joint twinning- and transformation-induced plasticity in a metastable β titanium alloy [J]. Acta Materialia, 2018, 151: 67−77.

[28] CHEN Bin, SUN Wei. Transitional structure of $\{332\}\langle113\rangle\beta$ twin boundary in a deformed metastable β-type Ti−Nb-based alloy, revealed by atomic resolution electron microscopy [J]. Scripta Materialia, 2018, 150: 115−119.

[29] MIN Xiao-hua, EMURA S, ZHANG Ling, TSUZAKI K, TSUCHIYA K. Improvement of strength-ductility tradeoff in β titanium alloy through pre-strain induced twins combined with brittle ω phase [J]. Materials Science and Engineering A, 2015, 646: 279−287.

[30] ZHOU Wei, WANG Chang, LIU Ji-xiong, LI Si-yun, LIU Hui-qun. Ageing precipitation sequence and effect of ω and secondary α phases on tensile properties of metastable β Ti−6Cr−5Mo−5V−4Al alloy [J]. Transactions of Nonferrous Metals Society of China, 2023, 33: 1742−1754.

[31] MIN Xiao-hua, TSUZAKI K, EMURA S. Enhanced uniform elongation by pre-straining with deformation twinning in high-strength β-titanium alloys with an isothermal ω-phase [J]. Philosophical Magazine Letters, 2012, 92: 726−732.

[32] PILZ S, HARIHARAN A, GUNTHER F, ZIMMERMANN M, GEBERT A. Influence of isothermal omega precipitation aging on deformation mechanisms and mechanical properties of a β-type Ti−Nb alloy [J]. Journal of Alloys and Compounds, 2023, 930:167309−167318.

[33] WANG Jun-shuai, XIAO Wen-long, FU Yu, REN Lei, MA Chao-li. Dependence of mechanical behavior on grain size of metastable Ti−Nb−O titanium alloy [J]. Progress in Natural Science: Materials International, 2022, 32: 63−71.

[34] WILLIAMS J C, HICKMAN B S, MARCUS H L. The effect of omega phase on the mechanical properties of titanium alloys [J]. Metallurgical Transactions, 1971, 2: 1913−1919.

[35] SIKKA S K, VOHRA Y K, CHIDAMBARAM R. Omega phase in materials [J]. Progress in Materials Science, 1982, 27: 245−310.

[36] SUKEDAI E, HASHIMOTO H. Investigation of volume fraction of omega particles and hardness value of aged Ti−Mo alloy using dark-field TEM imaging [J]. Microscopy and Microanalysis, 1992, 50: 310−311.

[37] XIAO Jun-feng, NIE Zhi-hua, HE Bin-bin, TAN Cheng-wen. Interplay between dislocation glide and ω precipitation in a Ti−15Mo alloy investigated by TEM [J]. Materials Science and Engineering A, 2023, 870: 144855−144860.

[38] KOUL M K, BREEDIS J F. Omega phase embrittlement in aged Ti−V [J]. Metallurgical and Materials Transactions B, 1970, 1: 1451−1452.

[39] QIAN Bing-nan, LILENSTEN L, ZHANG Jin-yong, YANG Min, SUN Fan, VERMAUT P, PRIMA F. On the transformation pathways in TRIP/TWIP Ti−12Mo alloy [J]. Materials Science and Engineering A, 2021, 822: 141672−141681.

[40] NARTU M S K K Y, SHARMA A, MANTRI S A, HARIDAS R S, REN Yang, BANERJEE R. Increasing the yield strength while preserving strain hardenability and ductility in a beta titanium alloy exhibiting transformation induced plasticity (TRIP) [J]. Scripta Materialia, 2022, 219: 114890−114896.

[41] SHI Rong-pei, ZHENG Yu-feng, BANERJEE R, FRASER H L, WANG Yun-zhi. ω-assisted α nucleation in a metastable β titanium alloy [J]. Scripta Materialia, 2019, 171: 62−66.

[42] SHI Xiao-hui, ZHANG Qi, JING Zhen, FAN Zhi-yuan, LIU

Jiang-lin, QIAO Jun-wei. Strengthening behavior and model of ultra-high strength Ti−15Mo−2.7Nb−3Al−0.2Si titanium alloy [J]. Transactions of Nonferrous Metals Society of China, 2024, 34: 1136−1149.

[43] WU Chuan, ZHAN Mei. Effect of solution plus aging heat treatment on microstructural evolution and mechanical properties of near-β titanium alloy [J]. Transactions of Nonferrous Metals Society of China, 2019, 29: 997−1006.

[44] NAKANISHI D, KAWABATA T, AIHARA S. Brittle crack propagation resistance inside grain and at high angle grain boundary in 3% Si−Fe alloy [J]. Acta Materialia, 2018, 144: 768−776.

[45] MELLO D G M, DAINESE P B, CARAM R, CREMASCO A. Influence of heating rate and aging temperature on omega and alpha phase precipitation in Ti−35Nb alloy [J]. Materials Characterization, 2018, 145: 268−276.

[46] CHEN Wei, CAO Shuo, KOU Wen-juan, ZHANG Jin-yu, WANG Yue, ZHA You, SUN Jun. Origin of the ductile-to-brittle transition of metastable β-titanium alloys: Self-hardening of ω-precipitates [J]. Acta Materialia, 2019, 170: 187−204.

[47] XIAO Jun-feng, NIE Zhi-hua, LIU Guang-fa, HAO Fang, TAN Cheng-wen. ω precipitation: Deformation regulator in metastable titanium alloys [J]. Materials Science and Engineering A, 2020, 772: 138687−138698.

[48] MELLO D G M, SALVADOR A C, FANTON L, CARAM R. High strength biomedical Ti−13Mo−6Sn alloy: Processing routes, microstructural evolution and mechanical behavior [J]. Materials Science and Engineering A, 2019, 764: 138190−138199.

通过变形辅助调节等温 ω 析出以减弱亚稳 Ti−15Mo 合金的时效诱导脆化

张 飞[1,2]，潘士伟[1,2]，徐 舜[1,2]，钱 锋[1,2]，樊江昆[3]，范群波[1,2,4]，程兴旺[1,2]

1. 北京理工大学 材料科学与工程学院，北京 100081；
2. 冲击与冲击材料科学技术国家重点实验室，北京 100081；
3. 西北工业大学 凝固技术国家重点实验室，西安 710072；
4. 北京理工大学 重庆创新中心，重庆 401135

摘 要：为了克服亚稳钛合金时效过程中 ω_{iso} 相析出引起的脆化，研究了 Ti−15Mo 合金等温 ω 相的析出规律。结果表明，固溶处理试样在 350 ℃直接时效 1 h 后表现出脆性断裂特征。对固溶试样进行预变形以诱导{332}孪晶和次生 α''相形成，并随后在 350 ℃下时效(STDA350)可将强度提高到 931 MPa，并保持约 20 %的良好延展性。预变形试样在 400 ℃或 450 ℃进行时效时(STDA400/450)，强度可以进一步提高，但延展性会显著降低。原子尺度表征表明，STDA350 试样中 ω 相结构部分坍塌，有效消除了时效引起的脆化；但 STDA400/450 试样中 ω 相结构完全坍塌，导致延展性较差。

关键词：室温力学性能；结构坍塌；ω 相；时效脆化；Ti−15Mo 合金

(Edited by Bing YANG)